

SCIENTIFIC REPORTS



OPEN

A Dynamic Precision Evaluation Method for the Star Sensor in the Stellar-Inertial Navigation System

Jiazhen Lu, Chaohua Lei & Yanqiang Yang

Integrating the advantages of INS (inertial navigation system) and the star sensor, the stellar-inertial navigation system has been used for a wide variety of applications. The star sensor is a high-precision attitude measurement instrument; therefore, determining how to validate its accuracy is critical in guaranteeing its practical precision. The dynamic precision evaluation of the star sensor is more difficult than a static precision evaluation because of dynamic reference values and other impacts. This paper proposes a dynamic precision verification method of star sensor with the aid of inertial navigation device to realize real-time attitude accuracy measurement. Based on the gold-standard reference generated by the star simulator, the altitude and azimuth angle errors of the star sensor are calculated for evaluation criteria. With the goal of diminishing the impacts of factors such as the sensors' drift and devices, the innovative aspect of this method is to employ static accuracy for comparison. If the dynamic results are as good as the static results, which have accuracy comparable to the single star sensor's precision, the practical precision of the star sensor is sufficiently high to meet the requirements of the system specification. The experiments demonstrate the feasibility and effectiveness of the proposed method.

The inertial navigation system (INS), which can provide continuous and comprehensive navigation information of a carrier by using a gyro and an accelerometer, has been widely applied in military and civilian fields¹⁻³. However, navigation errors accumulate over time in this system as a result of many error sources, such as initialization error, inertial sensor bias and computational error. Therefore, other navigation approaches are necessary to mitigate these errors in INS⁴⁻⁸. With the development of optoelectronics and image-processing techniques, the star sensor based on a charge-coupled device (CCD) or complementary metal-oxide semiconductor (CMOS) has become an attitude measurement instrument with the highest accuracy⁹⁻¹¹. The star sensor offers many good characteristics: it is non-radiating, invulnerable to jamming and invariant to changes in time and distance, and it can obtain high-precision attitude information of a body in an inertial frame^{12,13}. Therefore, the stellar-inertial navigation system combines INS and the star sensor to take advantage of both their merits; indeed, the stellar-inertial navigation system is a promising combination for application to marine systems, military aircraft and deep-space exploration¹⁴⁻¹⁸. Because the accuracy of the star sensor, which can reach the arc-second level, directly determines the integrated navigation accuracy, verification of star sensor accuracy becomes an important step in stellar-inertial integration applications.

Many researchers have studied calibration and accuracy verification methods for the single star sensor¹⁹⁻²³. The standard procedure is that the accuracy of the star sensor is tested after the application of various calibration methods; in other words, the verification experiment aims to verify the presented calibration method and then demonstrates the accuracy of the star sensor. Various calibration algorithms, both ground-based and on-orbit, have been proposed to estimate the most effective values of the optical parameters of the star camera using least-squares estimation or another fitting method²⁴⁻²⁷. Then, laboratory simulations or real night-sky tests are implemented to evaluate the accuracy of the star sensor after parameter compensation and to further assess the performance of the calibration methods. Thomas developed a complete calibration and qualification process for the TERMA star tracker to test its performance²⁸. In addition, with the advanced development of the high-precision star simulator, the in-lab calibration accuracy of the single star sensor has improved dramatically^{29,30}. Regarding the accuracy evaluation method of the star sensor, Sun proposed an accuracy measurement method

The Science and Technology on Inertial Laboratory, School of Instrumentation Science and Opto-electronics Engineering, Beijing University of Aeronautics and Astronautics, Beijing, 100191, China. Correspondence and requests for materials should be addressed to J.L. (email: lizbuaa@163.com)

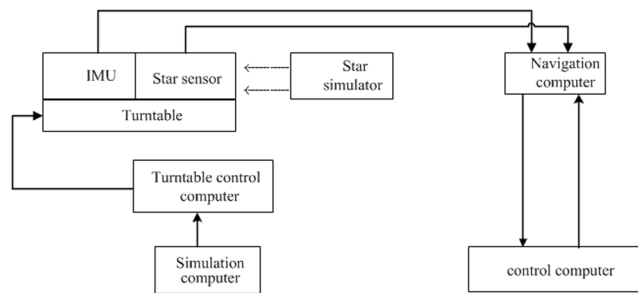


Figure 2. The experimental principle of calibration for the stellar-inertial integrated system.

- (3) The star sensor frame ($Ox_s y_s z_s$) has its origin at the center of the image plane of the star sensor with the optical axis (y -axis) pointing toward a star.
- (4) The computed navigation coordinate frame ($Ox_n y_n z_n$) is the local-level coordinate frame located at the computed position.

The transformation matrix from the star sensor coordinate frame to the geographic coordinate frame.

The proposed precision evaluation method employs the information generated from the star simulator, which is a high-precision reference value in the geographic coordinate frame, as the gold-standard reference. It is necessary to transform the starlight vector measured by the star sensor into the geographic coordinate frame. The transformation matrix from the measurement frame to the geographic frame can be obtained by the INS navigation solution using information from the gyro and accelerometer. Then, the transformation matrix from the body frame to the star sensor frame is also calculated. As a result, to improve the reliability of the proposed method, the first step is the precise calibration of the inertial sensor and installation errors between the star sensor and the body frame; the work principle of this process is shown in Fig. 2. This process is first conducted to confirm the error parameters of the sensors in the stellar-inertial navigation system.

The static precision evaluation of the star sensor. A high-precision star sensor, theoretically, has the same accuracy in a single instrument as a stellar-inertial navigation system. In addition, the static and dynamic precision in the integrated system should be comparable. Therefore, the static precision evaluation of the star sensor is implemented for comparison; the principal procedure is given in the following description.

In the proposed method, the gold-standard reference and the starlight vector measured by the star sensor are compared to calculate the errors. Obtaining the corresponding measurement information of celestial angles is the main objective of this integration algorithm. The differences in azimuth and elevation angles between the gold-standard reference and measurement by the star sensor are used as precision evaluation criteria, which can be written as

$$\delta El = El_c - El_n \quad \delta Az = Az_c - Az_n. \quad (1)$$

where Az_n and El_n are the azimuth and elevation angles in the geographic coordinate frame, respectively, Az_c and El_c are the azimuth and elevation angles calculated by star sensor in the computed navigation coordinate frame, respectively. They can be obtained by following steps.

- (1) The star simulator, which is mounted at a known position with precise orientation, can generate the gold-standard reference of the starlight vector in the geographic coordinate frame.

$$l_n = [x_n \quad y_n \quad z_n] \quad (2)$$

The starlight vector³⁹ is defined in terms of azimuth Az and elevation El relative to a reference frame ($O-xyz$), as shown in Fig. 3. The first rotation is about the z -axis through the Az angle, resulting in an intermediate frame $O-x_1 y_1 z_1$. Then, a rotation about x_1 through the El angle is performed to establish the starlight-vector axis in frame $O-x_2 y_2 z_2$.

The relationship between the starlight vector in the reference frame and the azimuth and elevation angles is written as

$$l = \begin{bmatrix} \sin Az \cos El \\ \cos Az \cos El \\ \sin El \end{bmatrix}. \quad (3)$$

Then, the azimuth and elevation angles in the geographic coordinate frame can be calculated by

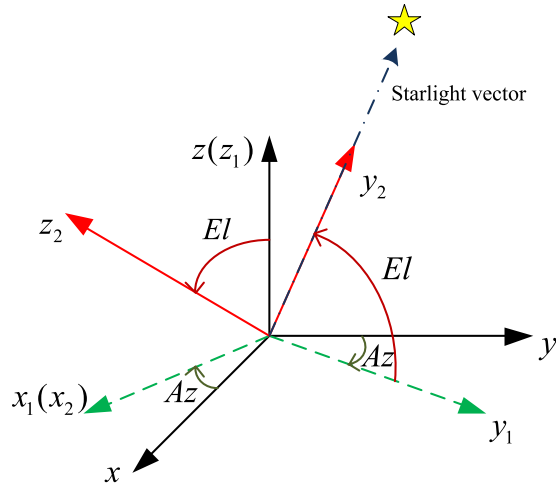


Figure 3. The definition of the azimuth and elevation angles.

$$\begin{aligned} El_n &= \sin^{-1}[I_n(3)] \\ Az_n &= \tan^{-1}\left[\frac{I_n(1)}{I_n(2)}\right]. \end{aligned} \tag{4}$$

- (2) Then, the El_c and Az_c can be calculated by the starlight vector in the computed navigation coordinate frame.

$$\begin{aligned} El_c &= \sin^{-1}[I_c(3)] \\ Az_c &= \tan^{-1}\left[\frac{I_c(1)}{I_c(2)}\right]. \end{aligned} \tag{5}$$

- (3) The starlight vector in the computed navigation coordinate frame can be calculated by

$$l_c = \tilde{C}_b^n l_b = [I - (\phi \times)] C_b^n l_b. \tag{6}$$

In this equation, l_b is the starlight vector in the body frame. INS can produce the attitude matrix \tilde{C}_b^n by navigation solution, but it contains attitude errors when compared with the true attitude matrix C_b^n .

$$\tilde{C}_b^n = [I - (\phi \times)] C_b^n \tag{7}$$

where ϕ is the attitude error.

- (4) The star sensor can detect the line of sight $\vec{l}_s = [x_s \ y_s \ z_s]$ from the star simulator, which contains static measurement error δ_{static} . Then the starlight vector in the body frame can be expressed as

$$l_b = C_s^b \vec{l}_s, \tag{8}$$

where C_s^b is the transformation matrix from the star-sensor frame to the body frame. In the first calibration step, three installation errors of the star sensor $[\mu_x \ \mu_y \ \mu_z]$ are estimated. Then, they are used to compute the transformation matrix C_s^b , which can be written as

$$C_s^b = \begin{bmatrix} \cos \mu_y \cos \mu_z - \sin \mu_y \sin \mu_x \sin \mu_z & \cos \mu_y \sin \mu_z + \sin \mu_y \sin \mu_x \cos \mu_z & -\sin \mu_y \cos \mu_x \\ -\cos \mu_x \sin \mu_z & \cos \mu_x \cos \mu_z & \sin \mu_x \\ \sin \mu_y \cos \mu_z + \cos \mu_y \sin \mu_x \sin \mu_z & \sin \mu_y \sin \mu_z - \cos \mu_y \sin \mu_x \cos \mu_z & \cos \mu_y \cos \mu_x \end{bmatrix}. \tag{9}$$

- (5) As a result, the starlight vector in the computed navigation coordinate frame³⁷ can be written as

$$l_c = \tilde{C}_b^n l_b = [I - (\phi \times)] C_b^n C_s^b \vec{l}_s. \tag{10}$$

It is seen from equation (10) that the influencing factors contributing to errors in l_c include attitude matrix error, installation errors of the star sensor and measurement error of the star sensor.

The measurement error of the star sensor δ_{static} is what the proposed precision evaluation method will calculate.

The impact of installation errors on the star sensor, $[\mu_x \ \mu_y \ \mu_z]$, has been decreased by the first calibration step and subsequent compensation.

The attitude matrix error of the inertial navigation solution can be written as

$$\dot{\phi} = \delta\omega_{in}^n + \phi \times \omega_{in}^n - \delta\omega_{ib}^n \quad (11)$$

where $\omega_{in}^n = \omega_{ie}^n + \omega_{en}^n$, ω_{ie}^n is the Earth-rate angular rotation vector in the navigation frame, ω_{en}^n is the navigation-to-Earth angular rotation vector in the navigation frame, and $\delta\omega_{ib}^n$ is the output error of the gyro.

According to the error propagation properties of the pure inertial navigation in short time⁴⁰, attitude errors are caused by three factors.

(a) Initial attitude errors ϕ_0

Initial attitude errors lead to attitude errors in the navigation solution because the calculation of inertial navigation is an integration process. Thus, in the proposed precision evaluation method, the initial attitude error is minimized by precise initial alignment using a turntable.

(b) Gyro errors

The mathematical error model of three gyros generally can be expressed by

$$\begin{bmatrix} \delta\omega_x \\ \delta\omega_y \\ \delta\omega_z \end{bmatrix} = \begin{bmatrix} \delta S_x & E_{xy} & E_{xz} \\ E_{yx} & \delta S_y & E_{yz} \\ E_{zx} & E_{zy} & \delta S_z \end{bmatrix} \begin{bmatrix} \omega_x \\ \omega_y \\ \omega_z \end{bmatrix} + \begin{bmatrix} \varepsilon_x \\ \varepsilon_y \\ \varepsilon_z \end{bmatrix} + \begin{bmatrix} w_{gx} \\ w_{gy} \\ w_{gz} \end{bmatrix}, \quad (12)$$

where $\delta\omega_i$ is the output error of the gyro in the i -axis, $i = x, y, z$, ω_i is the input rotation rate of the gyro in the i -axis, δS_i is the scale-factor error of the gyro in the i -axis, E_{ij} is the misalignment of the gyro in the j -axis relative to the gyro in the i -axis, ε_i is the bias of the gyro in the i -axis, and w_{gi} is the random noise in the i -axis.

The gyro errors cause periodic oscillations of the attitude error. In an attempt to reduce this error source, precise calibration is performed to determine all constant errors, including bias, scale-factor errors and misalignments. Then, the results of the calibration are used to compensate outputs of gyros in real time.

(c) Accelerometer errors

Similarly, the mathematical error model of accelerometers can be given by

$$\begin{bmatrix} \delta f_x \\ \delta f_y \\ \delta f_z \end{bmatrix} = \begin{bmatrix} \delta K_x & M_{xy} & M_{xz} \\ M_{yx} & \delta K_y & M_{yz} \\ M_{zx} & M_{zy} & \delta K_z \end{bmatrix} \begin{bmatrix} a_x \\ a_y \\ a_z \end{bmatrix} + \begin{bmatrix} \nabla_x \\ \nabla_y \\ \nabla_z \end{bmatrix} + \begin{bmatrix} w_{ax} \\ w_{ay} \\ w_{az} \end{bmatrix}, \quad (13)$$

where δf_i is the output error of the accelerometer in the i -axis, $i = x, y, z$, a_i is the input acceleration rate in the i -axis, δK_i is the scale-factor error of the accelerometer in the i -axis, M_{ij} is the misalignment of the accelerometer in the j -axis relative to the accelerometer in the i -axis, ∇_i is the bias of the accelerometer in the i axis, and w_{ai} is the random noise in the i -axis.

The accelerometer errors can cause velocity errors and sequentially determine the ω_{en}^n error. It is same with gyro calibration: the calibration constant errors of the accelerometer are used to remove output errors.

Through the above error analysis, it is determined that the error sources impacting the measured starlight vector information on the navigation system are the star sensor measurement error and random noise after the first calibration step and initially precise alignment.

The dynamic precision evaluation of the star sensor. In static precision evaluation, the star sensor captures the line of sight when the system is stationary. In practical applications, the stellar-inertial integrated system sometimes requires measurement information from the star sensor under in-motion conditions. Therefore, the dynamic precision evaluation of the star sensor is also necessary to verify its dynamic measurement precision in a dynamic application environment. The principle of dynamic precision evaluation is the same as that of static precision evaluation. The output error of the star sensor, which contains dynamic measurement errors $\delta_{dynamic}$, can be evaluated.

Results

An experiment in the laboratory is conducted to validate the feasibility of the proposed method. The stellar-inertial navigation system under investigation includes a star sensor and an IMU consisting of three ring-laser gyroscopes (RLGs) and three quartz flexible accelerometers (QFAs). The update rate of the IMU is 100 Hz. The star sensor is mounted parallel to the body coordinate frame and the optical axis is aligned with the y body axis. The accuracy of the star sensor is $3''$ (3σ) in the star sensor coordinate frame and its update rate is 10 Hz. The two most important pieces of equipment are the star simulator and three-axis turntable. The three-axis turntable is able to rotate the integrated system to different positions with high accuracy. Three star simulators are mounted in the east, north, and upward directions of the turntable. The parameters and accuracy of the star simulator are as follows: the star-pointing accuracy is $0.5''$ (3σ); it can simulate the star magnitude of 1; and the field of view is $6^\circ \times 6^\circ$. When the star sensor is rotated to align the optical axis with the star simulator, the bright light is measured to generate starlight vectors.

Number	Attitude before rotation			Rotation angle(°)/ rotation axis
	y	z	x	
1	Xg	Yg	Zg	+90/Y
2	Xg	Zg	-Yg	+90/Y
3	Xg	-Yg	-Zg	+90/Y
4	Xg	-Zg	Yg	+90/Y
5	Xg	Yg	Zg	+90/Z
6	-Zg	Yg	Xg	+90/X
7	Yg	Zg	Xg	+90/X
8	Zg	-Yg	Xg	+180/X
9	-Zg	Yg	Xg	+90/Z
10	-Xg	Yg	-Zg	+180/Z

Table 1. The designed 10-position rotations of the calibration trajectory.

Accelerometer error											
Bias (μg)			Scale factor (ppm)			Misalignments ($''$)					
∇_x	∇_y	∇_z	δK_x	δK_y	δK_z	M_{xy}	M_{xz}	M_{yz}	M_{yz}	M_{zx}	M_{zy}
-46.7	-24.0	-40.1	1.5	-32.5	18.3	140.3	-287.3	-123.8	113.0	314.8	-215.7
Gyroscope error									Star-sensor error		
Bias ($^{\circ}/\text{h}$)			Scale factor (ppm)			Misalignments ($''$)			Installation error ($''$)		
ε_x	ε_y	ε_z	δS_x	δS_y	δS_z	E_{xy}	E_{xz}	E_{yz}	μ_x	μ_y	μ_z
0.06	0.03	0.04	6.2	25.5	5.8	-453.7	-35.7	-415.5	195.2	160.7	83.7

Table 2. Estimated results of IMU and the star sensor.

According to the aforementioned outline of the proposed method, the precision evaluation experiment on the star sensor is divided into three steps.

Step 1: Calibration. The starlight vectors measured by the star sensor need to be transformed into the geographic coordinate frame to be compared with the gold-standard reference. Moreover, the transformation of the attitude matrix is provided by INS. Therefore, the calibration of the stellar-inertial integrated system is first implemented to determine the installation errors of the star sensor and the constant errors of the IMU, to further improve the precision evaluation performance. To increase the system observability, a sequential 10-position rotation is designed for the stellar-inertial navigation system to calibrate all sensor errors. The calibration trajectory is given in Table 1. Xg, Yg, and Zg represent east, north, and up in the local geographic coordinate frame.

Based on the observability analysis, the calibration trajectory can estimate bias, scale-factor error and misalignments of IMU and installation errors of the star sensor. Table 2 presents the final estimated values of all sensor errors.

As shown in the Table 1, the estimated biases of the gyros and accelerometers are ($0.06^{\circ}/\text{h}$, $0.03^{\circ}/\text{h}$, $0.04^{\circ}/\text{h}$) and ($-46.7\mu\text{g}$, $-24\mu\text{g}$, $-40.1\mu\text{g}$), respectively. If they are not calibrated, the influence on the navigation solution is large; furthermore, the precision evaluation results of the star sensor are affected by other factors in addition to the measurement error of the star sensor. The three installation errors of the star sensor are $195.2''$, $160.7''$ and $83.7''$, which are much larger than the accuracy of the star sensor, $3''$. Thus, it is of great importance to calibrate and compensate for the installation errors of the star sensor.

In the navigation solution process, the outputs of the gyros and accelerometers are compensated for utilizing the estimates of sensor errors, thereby improving navigation accuracy. The transformation matrix is calculated using equation (5) to compensate for the star sensor output.

Step 2: Static precision evaluation of the star sensor. The measurement precision of a single position is not sufficient to validate the performance of the star sensor. In a real situation, systems complete some motion and then utilize the star sensor to perform observations under stationary conditions. For this reason, a sequential 10-position rotation, given in Table 3, is designed to verify the static precision of the star sensor. The rotation rate is set as $9^{\circ}/\text{s}$ and each position is maintained for 30 seconds. The entire process lasts 5 minutes. For the static test, the system is stationary for 20 seconds and the star sensor measures the line of sight in the last 5 seconds, and then it takes 10 seconds to rotate to the next position. In this experiment, the optical axis of the star sensor is the y-axis and three simulators are mounted in the east, north, and up directions, respectively. There are 7 positions at which the optical axis aligns with the star simulators, to use measurement information for precision evaluation. It is clear that the starlight vectors of the fifth position and the ninth position are pointed upward. According to the relationship between the starlight vector and celestial angles, it can be deduced that the azimuth angles at these two positions are arbitrary. Consequently, the azimuth angles at these two positions are not computed for precision evaluation. To prove the repeatability and stability, 6 groups of static experiments are performed.

Number	Attitude before rotation			Rotation angle(°)/ rotation axis
	x	y	z	
1	Zg	Xg	Yg	+90/Y
2	Yg	Xg	-Zg	-90/Z
3	-Xg	Yg	-Zg	-90/Z
4	-Yg	-Xg	-Zg	+90/X
5	-Yg	Zg	-Xg	+90/Z
6	-Zg	-Yg	-Xg	+90/X
7	-Zg	Xg	-Yg	+90/X
8	-Zg	Yg	Xg	+90/Z
9	Yg	Zg	Xg	-90/Z
10	Zg	-Yg	Xg	+90/X

Table 3. The designed 10-position rotations of the evaluation trajectory.

Number	Extremum	Elevation angle errors at every position (″)							3 σ
		Position1	Position2	Position3	Position5	Position7	Position8	Position9	
1	Max	2.59	3.79	2.83	-0.26	2.06	2.49	-0.57	3.32
	Min	-2.25	-3.51	-3.14	-4.24	-2.75	-2.23	-3.95	
2	Max	3.32	2.91	3.72	-0.19	3.93	3.68	-0.87	3.58
	Min	-2.84	-3.58	-2.96	-3.84	-3.62	-4.31	-3.8	
3	Max	3.29	2.68	4.36	-0.37	3.58	3.91	-0.93	4.06
	Min	-2.91	-4.05	-3.62	-3.29	-2.84	-4.35	-3.25	
4	Max	3.61	3.92	2.88	-1.02	4.38	3.46	-0.39	4.13
	Min	-3.26	-2.68	-3.92	-3.99	-3.81	-4.05	-2.99	
5	Max	4.25	3.46	3.59	-0.98	2.86	3.48	-0.58	3.69
	Min	-3.31	-3.25	-4.12	-2.49	-3.53	-2.79	-4.34	
6	Max	4.23	4.05	3.51	-0.09	2.46	4.16	-0.19	3.83
	Min	-3.30	-3.52	-4.19	-4.32	-3.62	-3.08	-2.84	

Table 4. The elevation angle errors of static precision evaluation.

Number	Extremum	Azimuth angle errors at every position (″)					3 σ
		Position1	Position2	Position3	Position7	Position8	
1	Max	2.37	3.39	3.65	2.68	4.01	3.46
	Min	-2.99	-3.15	-2.35	-2.67	-3.58	
2	Max	4.29	2.94	3.79	3.94	3.61	3.57
	Min	-2.35	-3.51	-2.97	-3.65	-4.33	
3	Max	3.28	2.69	4.35	3.52	3.91	4.02
	Min	-2.91	-4.06	-3.63	-2.86	-4.35	
4	Max	3.65	3.54	2.85	4.32	2.94	4.26
	Min	-3.28	-4.21	-3.91	-3.86	-4.09	
5	Max	4.25	3.86	3.56	2.87	3.79	3.72
	Min	-3.32	-3.75	-4.10	-3.53	-3.84	
6	Max	3.56	2.98	3.52	2.57	3.48	3.91
	Min	-2.51	-3.53	-4.08	-3.72	-4.21	

Table 5. The azimuth angle errors of static precision evaluation.

Using accurate starlight vector information provided by the star simulator as the gold-standard reference, the azimuth and the elevation errors of star sensor measurement are computed and provided in Tables 4 and 5.

Tables 4 and 5 give the positive maximum and negative maximum of celestial angle errors at every position of every group experiment. It can be seen that the azimuth and the elevation errors have good consistency and stability. The 3-standard-deviation values (3 σ) of the celestial angle errors are calculated using all data of all observation positions in every group experiment. There are 50 points at every position. The 3 σ values of elevation errors in 6 groups of experiments are 3.32″, 3.58″, 4.06″, 4.23″, 3.69″, and 3.83″, and the 3 σ values of azimuth errors in 6 groups of experiments are 3.46″, 3.57″, 4.02″, 4.26″, 3.72″, and 3.91″. Based on the experimental results, it is

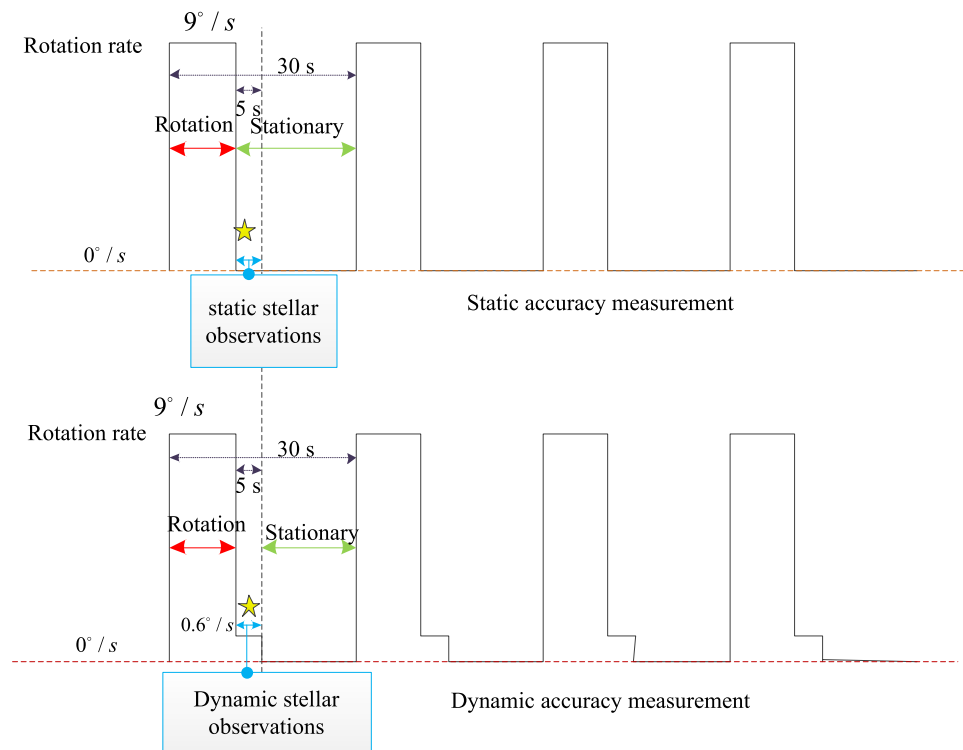


Figure 4. Comparison between static and dynamic experiments.

Number	Extremum	Elevation angle errors at every position (//)							3σ
		Position1	Position2	Position3	Position5	Position7	Position8	Position9	
1	Max	4.17	3.47	5.05	-0.06	3.13	5.32	-0.05	4.96
	Min	-3.43	-4.41	-3.61	-5.76	-2.75	-6.79	-6.76	
2	Max	5.48	5.24	6.25	-0.09	4.53	5.62	-0.12	5.58
	Min	-4.25	-3.93	-5.64	-5.91	-3.19	-4.78	-6.35	
3	Max	6.02	4.53	5.32	-0.18	5.64	5.06	-0.26	5.12
	Min	-3.96	-6.25	-4.16	-5.71	-4.93	-6.35	-5.45	
4	Max	4.86	4.56	6.19	-0.54	4.96	4.33	-0.49	4.83
	Min	-3.87	-3.94	-4.58	-4.69	-3.06	-3.98	-4.95	
5	Max	3.89	5.46	6.49	-0.62	4.39	6.23	-0.18	5.82
	Min	-5.26	-5.09	-4.76	-6.16	-3.61	-5.76	-6.39	
6	Max	4.96	6.14	5.63	-0.54	3.91	6.51	-0.61	6.08
	Min	-5.73	-3.83	-6.46	-4.52	-3.46	-5.49	-5.18	

Table 6. The elevation errors of dynamic precision evaluation.

concluded that the static precision of the star sensor is approximately 4", which is comparable to that of the single star sensor, 3". This result can be explained by the fact that the calculation is still affected by the small residual errors of IMU and the experimental environment noise, according to the above error analysis. In summary, the static precision evaluation results of the star sensor in the stellar-inertial integrated system prove that the static accuracy of the star sensor in experiments is high.

Step 3: Dynamic precision evaluation of the star sensor. The dynamic tests employ the same rotation trajectory as the static tests for comparison, as shown in Fig. 4. The difference is that the static accuracy measurement experiment measures the line of sight under stationary conditions, whereas the dynamic accuracy measurement experiment measures the line of sight with a rotation rate of 0.6°/s in the last 5 seconds. Both experiments move from the present position to the next position with a rotation rate of 9°/s. Hence the precision of the star sensor is evaluated in motion at the same position as under the static conditions. Six groups of dynamic precision evaluation experiments are also conducted, and the results are presented in Table 6 and Table 7.

From the given positive maximum and negative maximum of the celestial angle errors at every position of every group experiment, it can be concluded that the azimuth and the elevation errors also have good consistency

Number	Extremum	Azimuth angle errors at every position (″)					3σ
		Position1	Position2	Position3	Position7	Position8	
1	Max	3.97	5.68	5.46	5.69	4.85	5.06
	Min	-4.89	-5.05	-4.01	-5.76	-3.99	
2	Max	4.28	6.16	6.18	5.46	5.94	5.67
	Min	-5.49	-4.86	-3.84	-4.15	-6.08	
3	Max	5.16	6.09	5.67	6.14	4.63	5.20
	Min	-3.59	-5.14	-3.91	-5.46	-4.82	
4	Max	4.29	5.49	5.16	6.08	4.38	4.98
	Min	-5.48	-5.06	-3.98	-5.32	-3.54	
5	Max	6.21	5.54	6.41	4.96	5.29	5.90
	Min	-5.48	-5.49	-5.67	-6.04	-4.69	
6	Max	5.42	6.14	4.57	6.59	5.64	6.13
	Min	-4.39	-5.42	-6.38	-5.18	-4.81	

Table 7. The azimuth errors of dynamic precision evaluation.

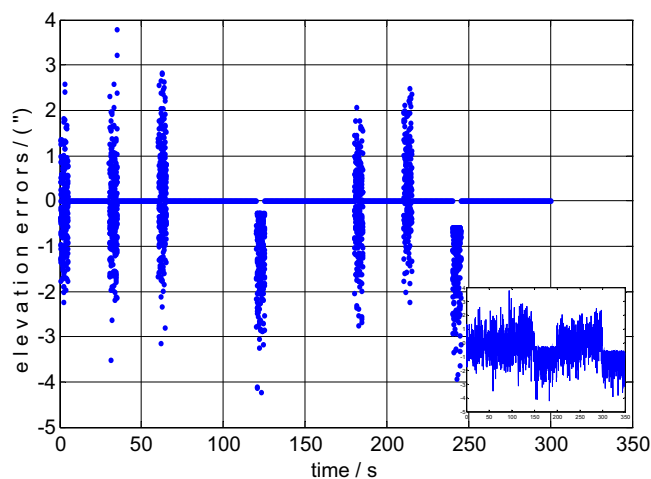


Figure 5. The static elevation errors of group 1.

and stability under motion. The 3σ values of the elevation errors in 6 groups of experiments are $4.96''$, $5.58''$, $5.12''$, $4.83''$, $5.82''$, and $6.08''$, and the 3σ values of the azimuth errors in 6 groups of experiments are $5.06''$, $5.67''$, $5.20''$, $4.98''$, $5.90''$, and $6.13''$. The experimental results show that the dynamic precision of the star sensor is approximately $6''$ compared with the static precision of $4''$, which proves the comparative accuracy. This result can be explained by the fact that the calculation is still affected by the small residual errors of IMU and dynamic noise according to the above error analysis. In sum, the dynamic precision evaluation results of the star sensor in the stellar-inertial integrated system prove that the dynamic accuracy of the star sensor in the experiment is as high as the static precision.

Discussion

Both the static and dynamic precision evaluation experiments are implemented in this section. The precision evaluation results for one of the 6 groups are depicted in Figs 5, 6, 7 and 8. There are 50 points of celestial angle error for 5 seconds at every position. It is clearly shown that dynamic and static celestial angle errors have consistent characteristics at every position. In addition, the dynamic error is only slightly larger than the static error. From the results of all 6 groups, it is determined that the static precision of the star sensor is approximately $4''$ and the dynamic precision is approximately $6''$. They are slightly larger than accuracy of the single star sensor of $3''$ due to residual IMU errors and noise, according to the above error analysis, but they have the same order of magnitude, from which the conclusion can be drawn that the precision of the star sensor in the stellar-navigation integrated system is high. It is reasonable that the dynamic measurement error $\delta_{dynamic}$ is larger than the static measurement error δ_{static} because of the image motion question under dynamic situations.

The results of the experiment show the practicability and feasibility of the proposed method in practice, whose main advantages are listed as follows:

- The existing method for precision evaluation of the star sensor is aimed at the instrument level. However, when the star sensor is applied to the stellar-inertial integrated system, evaluating its performance in the integrated system is essential to guarantee sufficient precision in the navigation process.

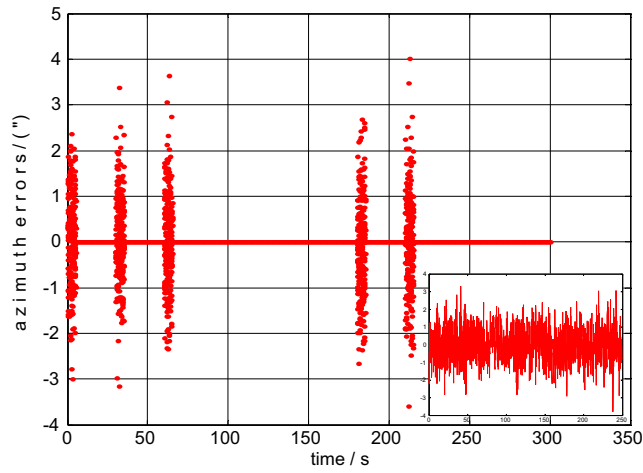


Figure 6. The static azimuth errors of group 1.

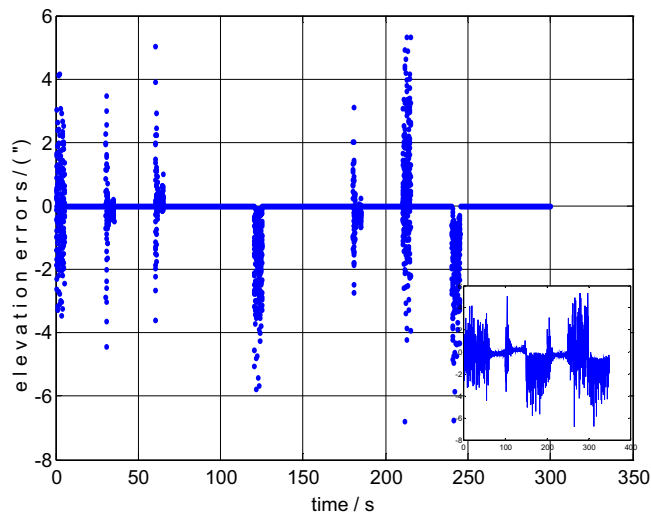


Figure 7. The dynamic elevation errors of group 1.

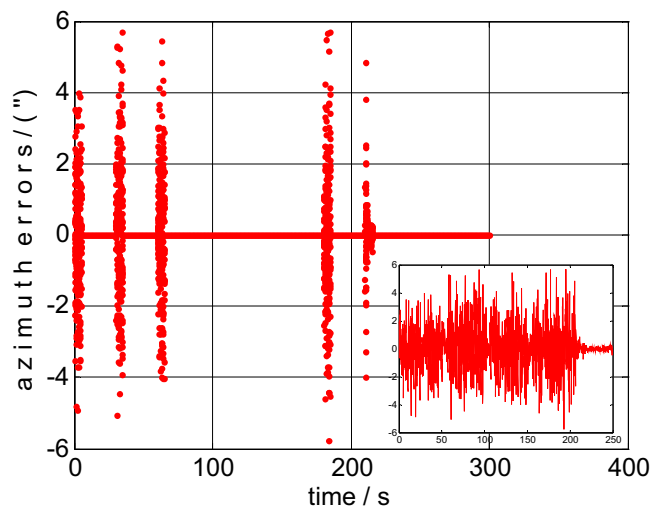


Figure 8. The dynamic azimuth errors of group 1.

- The proposed method first calibrated all sensor errors to be used for compensation in the subsequent precision evaluation experiment, which greatly diminished the influence of IMU errors and installation errors of the star sensor on the experimental results.
- The dynamic precision evaluation for the star sensor utilized the static precision results for comparison under the same trajectory condition. Because the proposed method employed the inertial navigation results, the static and dynamic precision evaluations are performed under the same environment and condition. Moreover, IMU outputs are compensated for using the same parameters.

There is a note that the proposed method is effective for any dynamic situation. In the experiments, the rotation rate is $0.6^\circ/s$ due to that the maximum dynamic range of the used star sensor is $0.6^\circ/s$. Beyond this value, the precision of star sensor will decrease. In the practical application, the rotation rate can be any value if the dynamic range of the star sensor is high.

In the practical application of the proposed method, if the dynamic precision evaluation result is the same order of magnitude as the static results, whose precision is comparable to the instrument-level accuracy of the star sensor, it demonstrates that the precision of the star sensor in the stellar-inertial integrated system is sufficiently high for navigation. By contrast, the limitation of the proposed method is that the dynamic accuracy of the star sensor cannot be declared poor if the precision evaluation results are considerably larger than the instrument-level accuracy of the star sensor. The existing problems need to be determined from the whole stellar-inertial integrated system.

Conclusions

The stellar-inertial navigation system has gained popularity in navigation applications such as airborne systems and missiles. In this paper, a dynamic precision evaluation method for the star sensor in the stellar-inertial integrated system is proposed. The star vector measured by the star sensor is transformed into the navigation frame through the attitude transformation matrix provided by the inertial navigation solution, whose accuracy is enhanced by first-step calibration for sensor errors. Utilizing the information of the star simulators as the gold-standard reference, elevation and azimuth angle errors in the geographic frame are calculated as precision evaluation criteria. Moreover, the static precision evaluation of the star sensor is also performed under the same evaluation trajectory condition with dynamic experiments for comparison. Regarding the star sensor used in the experiments, its static and dynamic precisions in the stellar-inertial integrated system are approximately $4''$ and $6''$, respectively, compared to the accuracy of the single star sensor of $3''$. The analysis of static and dynamic experiments shows the feasibility and stability of the proposed method in actual practice, which can be used for evaluating the arc-second-level star sensor.

References

1. Morgado, M., Oliveira, P., Silvestre, C. & Vasconcelos, J. F. Vehicle Dynamics Aiding Technique for Usbl/Ins Underwater Navigation System. *IEEE T Contr Syst T.* **22**, 111–116 (2014).
2. Sebesta, K. D. & Boizot, N. A Real-Time Adaptive High-Gain EKF, Applied to a Quadcopter Inertial Navigation System. *IEEE T Ind Electron.* **61**, 495–503 (2014).
3. Lu, J., Lei, C., Li, B. & Wen, T. Improved Calibration of IMU Biases in Analytic Coarse Alignment for AHRS. *MEAS Sci Technol.* **27**, 75105 (2016).
4. Chen, Y., Zhao, S. & Farrell, J. A. Computationally Efficient Carrier Integer Ambiguity Resolution in Multiepoch GPS/INS: A Common-Position-Shift Approach. *IEEE T Contr Syst T.* **24**, 1–16 (2015).
5. Hescht, J. A., Kottas, D. G., Bowman, S. L. & Roumeliotis, S. I. Consistency Analysis and Improvement of Vision-Aided Inertial Navigation. *IEEE T Robot.* **30**, 158–176 (2016).
6. Wu, Y., Wang, J. & Hu, D. A New Technique for INS/GNSS Attitude and Parameter Estimation Using Online Optimization. *IEEE T Signal Proces.* **62**, 2642–2655 (2014).
7. Gao, Z., Shen, W., Zhang, H., Niu, X. & Ge, M. Real-Time Kinematic Positioning of INS Tightly Aided Multi-GNSS Ionospheric Constrained PPP. *Sci Rep-UK.* **6**, 30488 (2016).
8. Zhang, X., Lin, Z. & Zhang, C. Autonomous Integrated Navigation Method Based On the Strapdown Inertial Navigation System and Lidar. *Opt Eng.* **53**, 990–999 (2014).
9. Cos, S., Uwaerts, D. & Hermans, L. Evaluation of STAR250 and STAR1000 CMOS Image Sensors. *J Appl Polym Sci.* **606**, 3–8 (2005).
10. Strikwerda, T. E., Fisher, H. L., Kilgus, C. C. & Frank, L. J. Autonomous Star Identification and Spacecraft Attitude Determination with CCD Star Trackers. *Spacecraft Guidance Navigation & Control Systems.* **1**, 195–200 (1991).
11. Wei, L. Optimum Designing of Baffle of CCD-star Sensor. *Missiles & Space Vehicles* (2002).
12. Liebe, C. C. Star Trackers for Attitude Determination. *IEEE Aerospace & Electronic Systems Magazine.* **10**, 10–16 (1995).
13. Aiaa & AIAA. Design of an APS Based Star Tracker for Microsatellite Attitude Determination. *AIAA J* (2004).
14. Ali, J., Zhang, C. & Fang, J. An Algorithm for Astro-Inertial Navigation Using CCD Star Sensors. *Aerospace Science & Technology.* **10**, 449–454 (2006).
15. Lu, J., Lei, C., Yang, Y. & Liu, M. A High-Accuracy Two-Position Alignment Inertial Navigation System for Lunar Rovers Aided by a Star Sensor with a Calibration and Positioning Function. *Meas Sci Technol.* **27**, 125102 (2016).
16. Wang, Q., Diao, M., Gao, W., Zhu, M. & Xiao, S. Integrated Navigation Method of a Marine Strapdown Inertial Navigation System Using a Star Sensor. *Meas Sci Technol.* **26**(250), 252 (2015).
17. He, Z., Wang, X. & Fang, J. An Innovative High-Precision SINS/CNS Deep Integrated Navigation Scheme for the Mars Rover. *Aerospace Science & Technology.* **39**, 559–566 (2014).
18. Zhang, L., Yang, H., Zhang, S., Cai, H. & Qian, S. Strapdown Stellar-Inertial Guidance System for Launch Vehicle. *Aerospace Science & Technology.* **33**, 122–134 (2014).
19. Lu, J. H., Wang, H. L., Wen, T. & Zhan, Q. L. Error Calibration Method for Star Sensor. *IEEE* (2011).
20. Xing, F., Dong, Y. & Zheng, Y. Laboratory Calibration of Star Tracker with Brightness Independent Star Identification Strategy. *Opt Eng.* **45**, 711–725 (2006).
21. Liu, H. & Hui, J. Novel Approach for Laboratory Calibration of Star Tracker. *opt Eng.* **49**, 3601 (2010).
22. Xing, F., Dong, Y. & You, Z. Laboratory calibration of star tracker with brightness independent star identification strategy. *Opt. Eng.* **45**, 063604 (2006).
23. Weng, J., Cohen, P. & Herniou, M. Camera calibration with distortion models and accuracy evaluation. *IEEE Trans. pattern Anal. Mach. Intell.* **14**, 965–980 (1992).

24. Sun, T., Xing, F. & You, Z. Optical system error analysis and calibration method of high-accuracy star trackers. *Sensors (Basel)*. **13**, 4598–4623 (2013).
25. Liu, H. & Jia, H. Autonomous On-Orbit Calibration of a Star Tracker Camera. *Opt Eng.* **50**, 68 (2011).
26. Rufino, G. & Moccia, A. Laboratory test system for performance evaluation of advanced star sensors. *J. Guid. Control Dyn.* **25**, 200–208 (2002).
27. Li, Y., Zhang, J., Hu, W. & Tian, J. Laboratory calibration of star sensor with installation error using a nonlinear distortion model. *Appl. Phys. B.* **115**, 561–570 (2014).
28. Paulsen, T. E. & Maresi, L. Calibration and verification of the TERMA star tracker for the NEMO satellite. *AIAA* **5338**, 1–8 (2000).
29. Zhao, C. G., Tan, J. B., Liu, J. & Wang, Y. H. Star Simulator for Testing Celestial Navigation Equipment. *Optics & Precision Engineering*. **18**, 1326–1332 (2010).
30. Airbus Defence and Space, STOS, Star Tracker stimulator. *Star-tracker-stimulator-8xa.html* (Accessed: 21th December 2015).
31. Sun, T., Fei, X., Wang, X., Zheng, Y. & Chu, D. An Accuracy Measurement Method for Star Trackers Based On Direct Astronomic Observation. *Sci Rep-UK*. **6** (2016).
32. Jørgensen, J. L., Jørgensen, P. S., Betto, M., Denver, T. & Tuñón, L. J. Enhanced mission performance from autonomous instrument guidance. *Acta Astronaut.* **59**, 981–989 (2006).
33. Yang, B., Wang, Y. & Qin, Y. Research On Autonomous Calibration On Orbit for the Integrated System of Strapdown Inertial Navigation System and Star Sensor. *Aerospace Control* (2010).
34. Egorov, S. N., Korabel'Shchikov, V. V. & Surinskii, D. M. Calibration of the Gyroinertial Meters of Attitude Control Systems Using Data From Stationary Star-Sighting Devices. *Mekhanika Tverdogo Tela*. **26** (1991).
35. Veth, M. J. & Raquet, J. F. Alignment and Calibration of Optical and Inertial Sensors Using Stellar Observations. Proceedings of International Technical Meeting of the Satellite Division of the Institute of Navigation. **45**, 165A (2007).
36. Hao, Y., Mu, H. & Liu, X. On-Line Calibration Technology for SINS/CNS Based On MPF-KF. *International Conference on Mechatronics and Automation*, 1132–1136 (2012).
37. Yang, G., Wang, L. & Yang, S. Online calibration method of missile-borne SINS/CNS integrated navigation system. *Journal of Projectiles, Rockets, Missile and Guidance*. **35**, 29–32 (2014).
38. Ma, L. *et al.* Attitude-Related Frames Approach for a Star Sensor to Improve Attitude Accuracy Under Highly Dynamic Conditions. *Appl Optics*. **54**, 7559–7566 (2015).
39. Kayton, M. & Fried, W. R. Avionics Navigation Systems. *Aerospace & Electronic Systems Magazine IEEE*. **12**, 12 (1969).
40. Rogers, R. M. *Applied Mathematics in Integrated Navigation Systems*, Third Edition. Reston American Institute of Aeronautics & Astronautics Inc. 78 (2015).

Author Contributions

Jiazhen Lu and Chaohua Lei designed the precision evaluation method; Jiazhen Lu, Yanqiang Yang and Chaohua Lei performed the experiments; Chaohua Lei and Jiazhen Lu wrote the paper; Jiazhen Lu and Chaohua Lei analyzed the data; all authors reviewed the manuscript.

Additional Information

Competing Interests: The authors declare that they have no competing interests.

Publisher's note: Springer Nature remains neutral with regard to jurisdictional claims in published maps and institutional affiliations.



Open Access This article is licensed under a Creative Commons Attribution 4.0 International License, which permits use, sharing, adaptation, distribution and reproduction in any medium or format, as long as you give appropriate credit to the original author(s) and the source, provide a link to the Creative Commons license, and indicate if changes were made. The images or other third party material in this article are included in the article's Creative Commons license, unless indicated otherwise in a credit line to the material. If material is not included in the article's Creative Commons license and your intended use is not permitted by statutory regulation or exceeds the permitted use, you will need to obtain permission directly from the copyright holder. To view a copy of this license, visit <http://creativecommons.org/licenses/by/4.0/>.

© The Author(s) 2017